Appl. Phys. A 69, 1–9 (1999)

Applied Physics A
Materials
Science & Processing

Diagnostics of laser-produced plume under carbon nanotube growth conditions

S. Arepalli[1,*], P. Nikolaev[1], W. Holmes[1], C.D. Scott[2]

[1] G.B. Tech./Lockheed Martin, 2400 NASA Road One, Mail Stop C61, Houston, TX 77058, USA
[2] NASA/JSC, 2101 NASA Road One, Mail Stop ES3, Houston, TX 77058, USA

Received: 17 May 1999/Accepted: 8 September 1999

Abstract. This paper presents diagnostic data obtained from the plume of a graphite composite target during carbon nanotube production by the double-pulse laser oven method. The in situ emission spectrum (300 to 650 nm) is recorded at different locations upstream of the target and at different delay times from the lasers (IR and green). Spectral features are identified as emissions from C_2 (Swan System: a $^3\Pi_g$–d $^3\Pi_u$) and C_3 (Comet Head System: A $^1\Pi_u$–X $^1\Sigma_u{}^+$). Experimental spectra are compared with computed spectra to estimate vibrational temperatures of excited state C_2 in the range of 2500 to 4000 K. The temporal evolution of the 510-nm band of C_2 is monitored for two target positions in various locations, which shows confinement of the plume in the inner tube and increase in plume velocity with temperature. The excitation spectra of C_2 are obtained by using a dye laser to pump the (0,1) transition of the Swan System and collecting the laser-induced fluorescence signal from C_2. These are used to obtain "ground-state" rotational and vibrational temperatures which are close to the oven temperature. Images of the plume are also collected and are compared with the spectral measurements.

PACS: 42.62.Fi; 81.05.Tp; 82.80.Ch

During recent years, there has been a tremendous increase in interest in the production and characterization of carbon nanotubes, due to their unique mechanical and electrical properties leading to potential applications in nanoelectronics [1, 2], nanostructures [3, 4], and energy storage [5, 6]. The most common nanotube production methods are arc, chemical vapor deposition, and laser ablation. The arc process has been in use for the last several years to produce both single-wall and multi-wall nanotubes (SWNTs and MWNTs). Recent work by Bernier's group [7] improved the yield of SWNTs in the arc process by using yttrium and nickel catalysts which helped initiate commercialization [8]. Chemical vapor deposition processes so far have yielded mostly MWNTs; and recent advances allow researchers to selectively deposit open or closed-end multi-wall tubes [9]. Also, there have been attempts to grow SWNTs by vapor phase chemical reactions of hydrocarbons and other carbon precursors [10]. Smalley and co-workers at Rice University developed the laser ablation method [11, 12] which yielded high purity SWNTs using a two-pulse YAG laser-oven technique. Recent work on the laser ablation method included other pulsed lasers (XeCl at 308 nm) [13] and cw lasers (diode-pumped YAG and CO_2) [14, 15].

A major obstacle to the growth of nanotube applications has been the low production rate of nanotubes. Therefore, it is important to study how nanotubes are formed, so that reasonable attempts can be made to scale up current efforts. The production mechanism and kinetics of production are not yet well understood. There have been some attempts to model the reactions in the arc process for producing C_{60} [16] and MWNTs in arcs [17]. Variation of parameters of the laser-oven method such as temperature of the oven [18], type of catalyst [19], and laser energy enabled production of specific types of SWNTs. Empirical variations of the parametric study at Rice University [11] have helped to optimize production rates and nanotube yield and purity. It was found that operating with two successive laser pulses, one at 532 nm followed 50 ns later by another at 1064 nm, resulted in the best yield. They also found that production is best at an argon pressure of about 67 kPa. The design and composition of the graphite target is also important for good production; a smooth target surface, and about 1% each of cobalt and nickel seem to be optimal. It has been speculated that the growth of nanotubes occurs from partially closed fullerenes held "open" by nano-sized particles of Co/Ni metal catalyst on which C_2 attaches. Since the feedstock is probably C_2 (or some other small molecular weight carbon clusters that condense out of vaporized carbon), this species can be monitored in the emission spectrum of the laser-produced ablation plume. This information can then be used as a gauge of how reactions leading to the formation of SWNTs might proceed kinetically. Unfortunately, there have been no known success-

*Corresponding author.
(E-mail: sivaram.arepalli1@jsc.nasa.gov)

MS ID: APA0251
6 January 2000 15:39 CET

ful attempts to measure the formation of SWNTs directly in situ.

Our group at NASA Johnson Space Center realized the need for a better understanding of the growth mechanism to improve the production process. Our goal was to study the production process and attempt to develop bulk methods for making nanotubes. It is believed that a study of this type will be useful in scaling up any process for commercial production. It will be difficult, at best, to produce large quantities of high quality SWNTs without a firm grasp of the mechanisms of formation. We have gathered information about the radiant species in the reaction area of the laser ablated plume [20] and conducted a preliminary parametric study. The data included spatial and transient spectral features of passive emission as well as laser-induced fluorescence of C_2 and C_3. The current paper focuses on the recent developments of the in situ diagnostics that included snapshots of plume images during nanotube production. The results of a parametric study that correlate spectral features with carbon nanotube yields will be presented later.

1 Experimental details

1.1 General setup

The apparatus for nanotube production by laser ablation, similar to the one used at Rice University [11], is shown in Fig. 1; and the details were presented at the NanoSpace 98 Conference in Houston, TX in November 1998 [21]. For the sake of completeness, some of the details are included here. The current configuration uses two lasers to ablate a graphite target containing cobalt and nickel (1 at. % each). The target is maintained at 1473 K in a tube furnace in argon atmosphere (100 sccm flow; 66.7 kPa pressure). Two 10-Hz high-power pulsed Nd:YAG lasers are used for the ablation process, operating at 1064 nm (IR) and 532 nm (green), each with 300-mJ pulse in a 5-mm beam. For normal operation, the IR laser pulse follows the green pulse by 50 ns. The laser beams are adjusted to travel colinearly onto an uncoated quartz right-angle prism and impinge on the target as overlapping beams. The prism mount is remotely controlled to generate a raster scan of the laser beams on the target to remove material uniformly from the target surface. The beam sizes are measured using a laser beam analyzer (Spiricon, LBA-300PC), and the pulse energies are measured using a volume-absorbing laser power meter.

1.2 Target and flow tube

The targets used for this study were supplied by Rice University and were made by compressing a paste containing high-purity graphite, metal catalysts, and Dylon^{TM} carbon cement and curing at high temperature (1073 to 1473 K) in a flowing argon atmosphere. The flow tube is a 56-mm-diameter quartz tube with a Brewster window on the front flange. The Brewster window flange also contains a 25-mm-diameter inner quartz tube and the laser beams are contained within this 25-mm clearance. The end flanges are water cooled, and a graphite ring is used to support the inner tube. Normally located about 6 mm from the end face of the inner tube, the end of the target moves to about 3 mm due to thermal expansion when the oven is heated to 1473 K. The target is located near the center of the oven. For normal operation, argon flow of 100 sccm at 66.7 kPa pressure is maintained in the inner tube using a MKS flow controller and throttle valve with PID controller.

1.3 Emission collection

Three optical fiber assemblies (Fig. 2) focus light from the central part of the ablation plume (Fig. 3) onto the end of an 800-μm quartz fiber attached to a Spex 270M spectrograph. Two detectors are used for recording the emission spectra: a gateable intensified CCD with 1024×256 pixels resolution (Princeton Instruments, 1024MLDG) and a photomultiplier tube (Hamamatsu Corp., R955). Two background

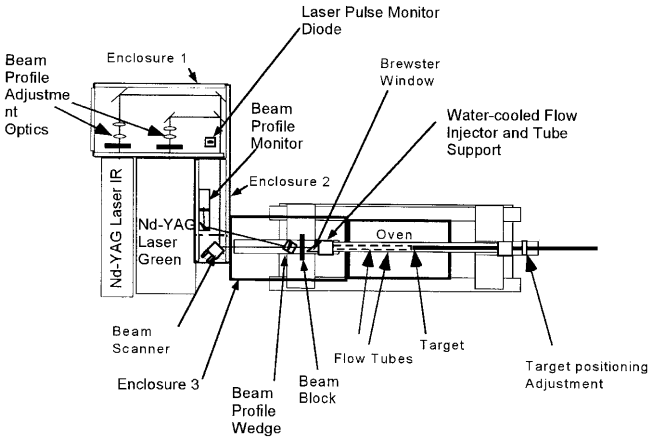

Fig. 1. Layout of the laser ablation process for single-wall nanotube production

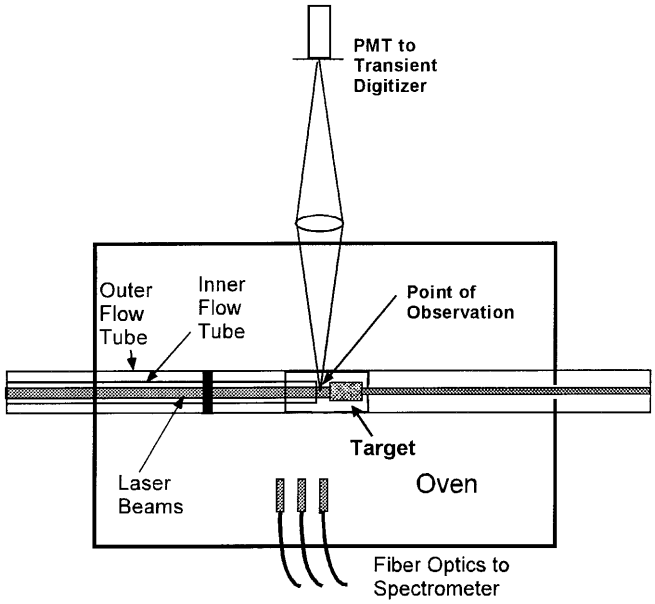

Fig. 2. Configuration of flow tubes and target showing laser beams, plume, fiber optic light collectors, and lens assembly for transient data collection

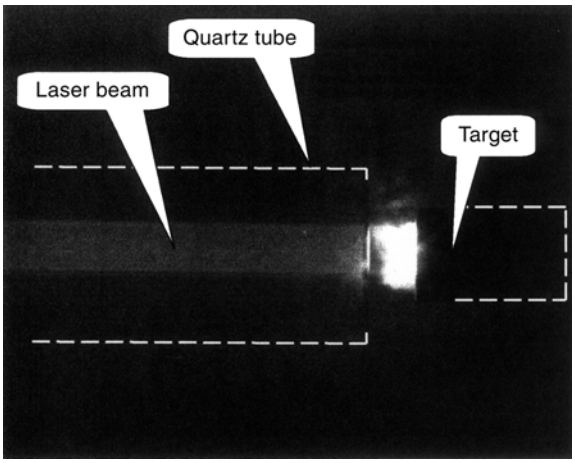

Fig. 3. Photograph of the target, plume, and laser-illuminated particles upstream in the inner tube

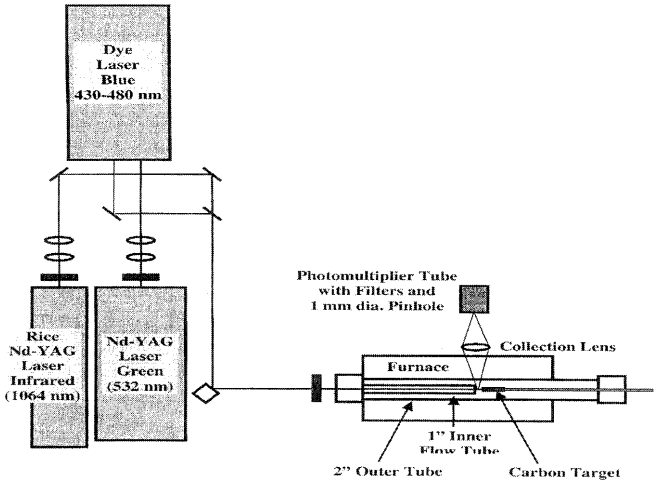

Fig. 4. Schematic of the LIF setup for plume diagnostics

signals were obtained with the same number of scans (100) as in the measured spectra. One was obtained before and the other after the spectral measurements and were averaged before subtracting them from the measured spectra. Most of the spectra are recorded with 25-μm slit widths using a 300-line/mm grating blazed at 500 nm. The resolution, taking into account the finite size of the intensifier channels, is about 1.9 nm. All the spectra are intensity calibrated using a standard lamp whose calibration is traceable to the NIST.

1.4 Transient data

Transient spectral data is collected by connecting the output of the R955 tube to a 32 K channel transient digitizer. The response time of the system can be as low as 3 ns and the estimated time resolution is about 20 ns. For better spatial resolution of the transient data, a lens and 1-mm pin-hole assembly are used to project the plume image (1:1) onto a R955 tube using a notch filter (Notch Plus from Kaiser Optical @532 nm), a wideband infrared blocking filter (KG5), and a narrow-band interference filter (510 nm) as shown in Fig. 2. All transient and steady-state data are collected with stationary laser beams at the center of the target. Data collection is initiated 90 s after ablation start to allow for thermalization of the target surface.

1.5 Laser-induced fluorescence (LIF) data

For LIF excitation scans, one of the two available YAG lasers is frequency-tripled to operate at 355 nm and is used to pump the tunable pulsed dye laser (Lambda Physik 3002E). This dye laser (435 to 475 nm) is then used to excite the (0,1) transitions of the C_2 Swan band system [22] in the plume region. With this arrangement, only the IR laser is available for ablating the carbon target, as shown in Fig. 4[TS a]. Two sets of LIF data are collected, one with a narrow-band (10 nm) interference filter centered at 510 nm to collect fluorescence from the $\Delta v = 0$ sequence region. The other set uses a long-pass filter to transmit wavelengths longer than 480 nm to collect $\Delta v = 0, -1, -2$ sequence bands of the Swan band system. Additionally, an IR filter (KG5) is positioned just behind the focusing lens to further reduce the IR coming from the hot plume region. The signal from the PMT is sent to a boxcar averager whose gate position and width is adjusted to pick out a small portion of the fast decaying LIF signal. Additionally, a second boxcar averager is used to measure the intensity of the dye laser pulses sampled by a photodiode, which is used to normalize the observed fluorescence intensities. A number of shots (ten) are then averaged before the dye laser is moved to the next wavelength step (step size = 0.00525 nm) in the scan. A plot of the LIF signal strength versus excitation wavelength then reveals several rotational peaks in the excitation scan which can be analyzed to yield relative density and temperature information.

1.6 Plume images

Images of the plume area are recorded by the ICCD detector equipped with a 85-mm Nikkor lens. A combination of three filters is used for image collection: an interference filter centered at 510 nm, a notch filter (532 nm) to block the scattered light from the green laser, and a KG5 filter to block the infrared. Several gate widths and time delays are used to map the plume area.

2 Observations and measurements

Five measurement techniques described in Sect. 2 are used for determining properties of the laser ablation process. These techniques are: (1) still and video photography; (2) wavelength-resolved emission spectroscopy; (3) transient spectral measurements; (4) excitation spectra using laser induced fluorescence of C_2, and (5) plume images obtained using the ICCD detector. Most of these measurements are obtained with the oven off (300 K) and at the nanotube production temperature of 1473 K.

2.1 Photographic observations

Photography was used to obtain estimates of the size and location of the visible plume which is confined to a small region

[TS a] Please supply new electronical data for Fig. 4.

Editor's or typesetter's annotations (will be removed before the final TEX run)

near the surface of the target. This plume extends about 1 cm from the surface and seems to have ragged edges. Its duration is very short, less than 1 μs per pulse, as confirmed first by high-speed video and then by transient emission measurements. The plume appears violet-white in color both from direct observation and from photographs. Figure 3 shows a close-up of the laser plume and part of the region inside the inner flow tube that is illuminated by the laser. This photograph was taken with a notch filter to remove scattered 532-nm laser radiation. It shows the luminous plume where high-temperatures exist. Inside the 1-inch tube in the region to the left of the plume, there is a glow that appears to contain high temperature particles, probably heated to incandescence by the lasers. The incandescence in the inner tube extends to about 7 cm as seen in Fig. 3. The recorded video shows complex flow patterns inside the incandescence area of the inner tube. Calculations of particle absorption of laser energy (taking into account the complex index of refraction of the particles) show that a large fraction of each particle may vaporize, particularly by the 532-nm beam.

2.2 *Passive emission spectral data*

The second diagnostic technique is wavelength-resolved emission spectroscopy. Spectra in the wavelength range of about 300 to 650 nm were collected with varying gate widths (0.05 to 100 μs) and at different delay times (0.1 to 300 μs). A typical set is shown in Fig. 5 with 10-μs gate width and different delays and laser combinations. The predominant feature in these spectra is the C_2 Swan band emission system that results from the transition $d\,^3\Pi_g$–$a\,^3\Pi_u$. We can see that for all times the single pulses produce much less radiation than the two lasers together. The effect is more than just additive. There seems to be a great synergism in intensity. This is consistent with production of carbon SWNTs, where the two-laser-pulse production rate is much greater than the sum of the single-pulse production rates. Apparently, the greater intensity of C_2 in the plume can be correlated with the production rate of SWNTs. Two sequential pulses probably heat the target to higher temperatures than a single pulse. Since the vapor pressure varies nonlinearly with temperature, we may expect greater ablation with two pulses than just "addition". The 50-ns delay between the two laser pulses seems to be an optimum, and may be related to a minimum of laser absorption by the plume before the target cools. We can see in Fig. 5 that as time progresses, the intensity of all plumes decreases. More will be discussed about the time evolution of the plumes in the following sections.

2.2.1 Variation with distance and time delay. Variation of the spectral intensity with distance from the target is shown in Fig. 6, where the optical fibers located at distances of 50 and 100 mm (fibers 2 and 3) collect light from the incandescence region in the inner tube. We have used large gate widths (100 μs) for this comparison. The peak intensity dropped off by a factor of 20 from fiber 1 to fiber 2, but leveled off at fiber 3. The spectral features with oven off (300 K) and oven on (1473 K) are similar, but the intensity increases by a factor of 20 with a hot oven. This is not attributable to movement of the target into the viewing area of the optical fiber at 1473 K.

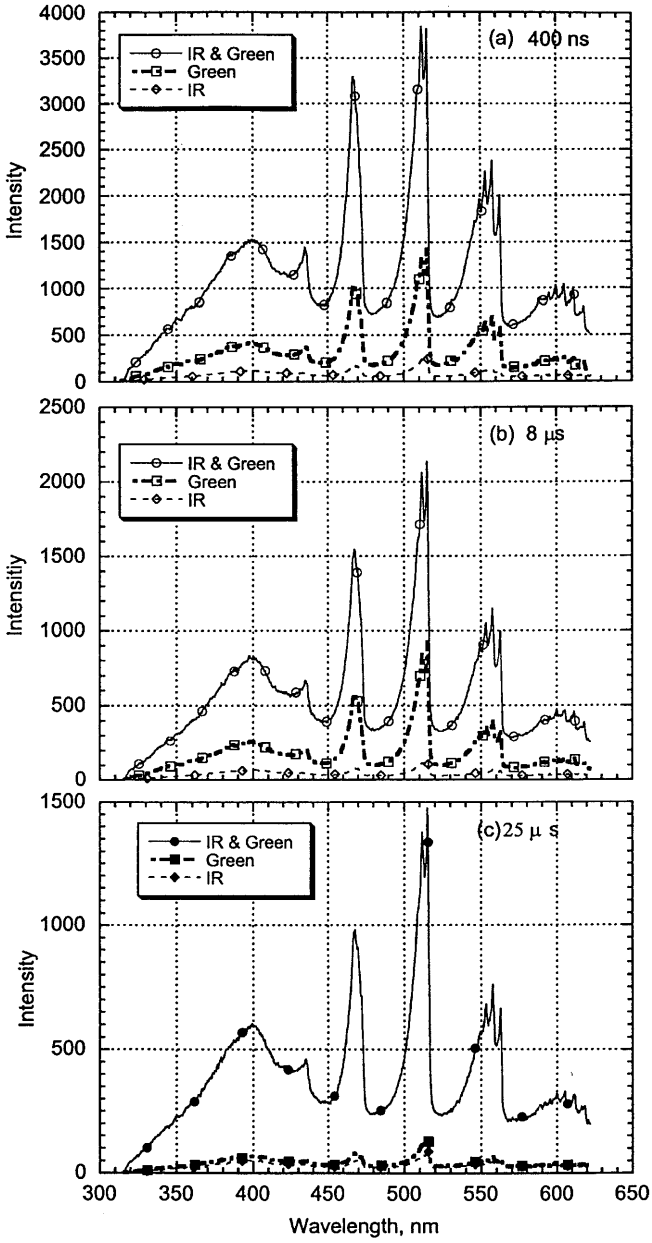

Fig. 5. Emission spectra taken at time delays of 0.4, 8, and 25 μs for all laser pulses

There is a considerable change in relative intensities of the Swan bands with delay time which is indicative of vibrational temperatures peaking at early times in the range of 2 to 5 μs. The spectral features in the short-wavelength range attributable to C_3 seem to start appearing after about 350 ns and plateauing at about 1000 ns. The appearance is clearly seen in Fig. 7 which shows the effect of increasing gate width (100 ns to 500 ns) at a fixed delay of 150 ns. Also, the background attributable to blackbody-like emissions has temporal behavior. There is a noticeable difference in the background which slopes up to long wavelengths for short delays (< 1 μs), levels off, and slopes back up to long wavelengths at longer delay times (> 50 μs). The higher intensity at longer wavelengths indicate blackbody-like emissions with temperatures of the order of 3000 K (Fig. 8). The short delay-time behavior seems to be simi-

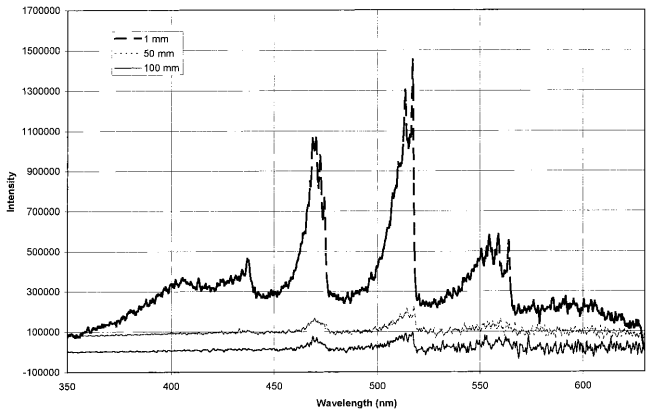

Fig. 6. Spectra collected by the three optical fibers located at different distances from the target during production run

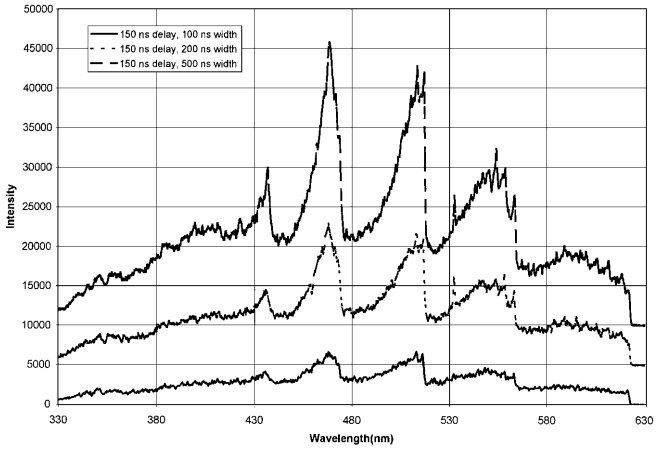

Fig. 7. Variation of spectra obtained with different gate widths (100, 200, 500 ns) with 150-ns time delay

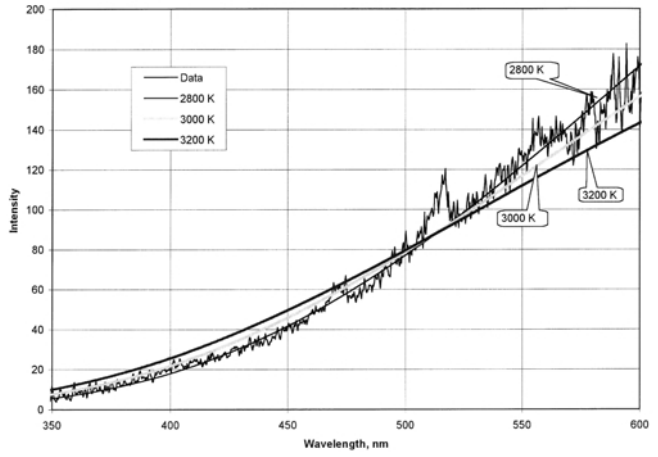

Fig. 8. Comparison of background continuum with black-body radiation for long delays

lar to that observed by Rohlfing [23] and the blackbody emission may involve the process of cooling of laser-heated particles.

We see an underlying continuum that has a maximum at about 400 nm that is not completely understood. The underlying continuum may be due to radiation from C_3 ($X\,^1\Sigma_g^+$–$A\,^1\Pi_u$), C_2 ($C\,^1\Pi_g$–$A\,^1\Pi_u$) and to particulate continua as discussed in our earlier paper [20].

2.2.2 Temperature estimation from emission analysis. Estimates of vibrational temperatures are possible for showing the relaxation of temperature with time. The ratio of vibrational peaks in the spectrum depends on the vibrational temperature. Using a technique described in [24], theoretical spectra were calculated at various temperatures, and ratios of integrals over short wavelength ranges were found as a function of temperature. In particular we chose to use the ratio of intensity integrals in the vicinity of the vibrational peaks (1,0) and (0,0) of the C_2 Swan band ($d\,^3\Pi_g$–$a\,^3\Pi_u$). The estimated vibrational temperatures ranged from 2500 to 4000 K [20]. These temperatures are calculated for a duration of 10 μs and therefore represent average values. The two-pulse operation may be responsible for these high plume temperatures. The surface temperature of the target may be greater with two close pulses leading to additional ablation. Yudasaka et al. [25] made measurements of nanotube production in a similar laser ablation facility at various pressures from about 0.5 kPa to about 67 kPa. They found that higher pressures resulted in increased production of carbon single-wall nanotubes. They proposed that this was due to greater evaporation of catalysts due to higher temperature surfaces at higher pressure. In the present experiments the two-laser pulse operation produces more SWNT, possibly because the surface temperature is higher. We also see that the C_2 Swan bands are much more intense, and therefore we attribute the increased production to a greater amount of carbon ablation. This does not necessarily contradict the conclusion of Yudasaka et al. [25] that evaporation of catalysts may be a factor in their experiments, since at our higher pressure, we were already in a regime in which nanotubes were produced for all laser combinations.

We have also attempted to subtract the continuum in the measurements for a better comparison with the calculated spectra. We see differences in the measured and calculated spectra at high vibrational/rotational energy levels toward the violet side of the band heads. The continuum was estimated by choosing the points at the minima between peaks in the Swan bands. These points were then curve fit and interpolated values were subtracted from the measured spectra. It was noted that the resultant spectra did not match calculated spectra over the entire wavelength range for any temperature. This indicates a nonequilibrium in the vibrational states. This may be due to high-level states being populated during C_2 formation rather than by thermal excitation. C_2 may be formed by recombination of carbon atoms (chemiluminescence) or by photodisoociation of larger carbon clusters. It is quite likely that the difference between measured and calculated spectra is due to dominance of the upper vibrational states during C_2 formation that leads to a nonequilibrium vibrational population. This hypothesis is also supported by the nature of the distribution of intensities in the $\Delta v = -1$ system in the wavelength range 530 to 565 nm and in the $\Delta v = -2$ system in the wavelength range 580 to 620 nm. Further investigation is warranted.

2.3 Transient emission measurements

Previous transient measurements of emission at various wavelengths associated with peaks in the spectra [20] were made using an optical fiber connected to the spectrometer. This includes a viewing column diameter of about 6 mm and the data could not be used for spatial resolution. The reported decay rates in [20] are probably overestimated because of larger viewing area. As mentioned in the experimental section, the spatial resolution is now reduced to 1 mm by using a lens and aperture combination.

In order to better understand the role of the inner tube in constraining the plume expansion and its effect on nanotube yield [12], we collected transient data at different distances from the target for two target positions. This was repeated for cold oven as well as hot oven. The data is shown in Figs. 9–12. The insets show the variation for early times. The second peak that comes at about 80 s shows very little intensity from C_2, with large contribution from blackbody-type emission (Fig. 8). In the case of hot oven, for the "normal" target distance of 3 mm from the inner tube (Fig. 9), the second peak does not seem to change in time for the distances of 0, 2, and 4 mm. There is a noticeable shift and spread in the peak for distances beyond 4 mm which indicates a velocity of about 50 m/s. When the target is moved back to be at 7 mm from the inner tube (Fig. 10), the transient data at long times seem to change dramatically. The intensity in the short times continually decreases and the second peak now seems to move uniformly with increasing distance. The velocity increases to about 75 m/s. These values seem to be corroborated by the recorded ICCD images discussed later in the paper. In the case of a cold oven, for the normal distance of 6 mm from the inner tube (Fig. 11), the intensity goes to essentially zero for distances greater than 4 mm, indicating smaller plume expansion. When the oven is cold, the velocity is about 25 m/s. However, when the target is moved back 10 mm from the inner tube (Fig. 12), there seems to be an increase in the plume size and its velocity increases to 40 m/s.

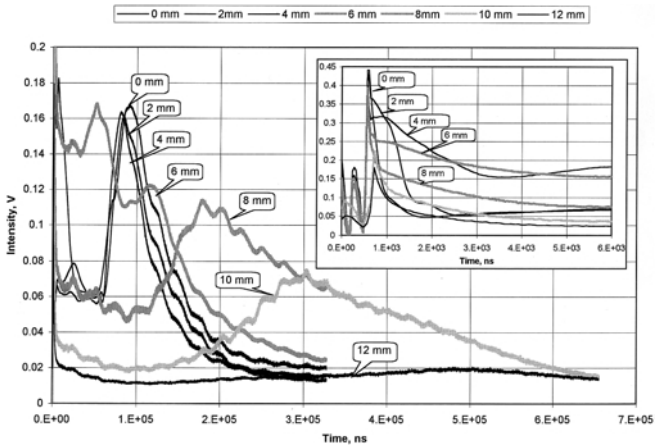

Fig. 9. Transient data with target at normal location of 3 mm from inner tube with PMT at different distances from the target; oven at 1473 K

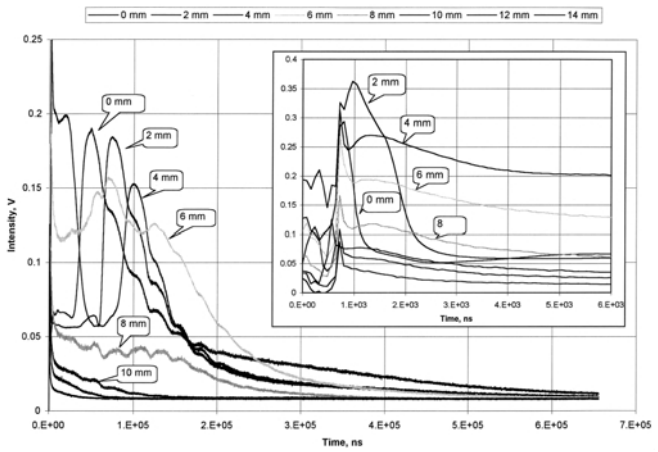

Fig. 10. Transient data with target at 7 mm from inner tube with PMT at different distances; oven at 1473 K

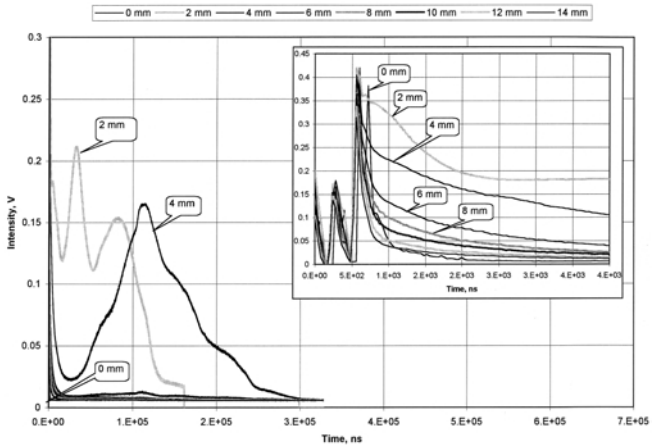

Fig. 11. Transient data with target at normal location of 6 mm with PMT at different distances; oven at 300 K

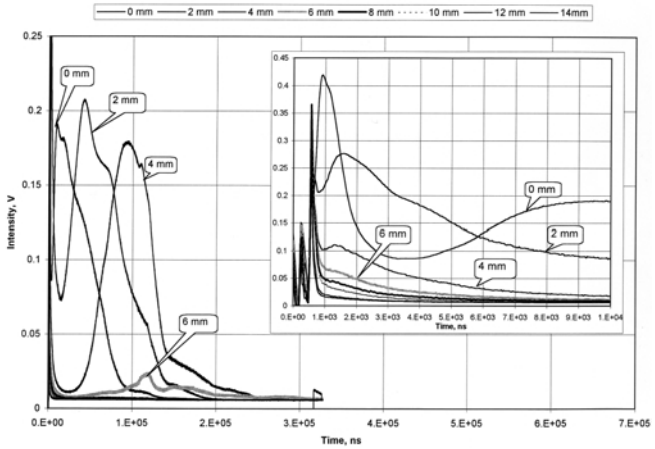

Fig. 12. Transient data with target at 10 mm from inner tube with PMT at different distances; oven at 300 K

2.4 LIF measurements

Excitation spectra of C_2 (471 to 474 nm) are obtained by pumping C_2 Swan bands in the (0,1) transition at about 473 nm and collecting fluorescence at longer wavelengths to include $\Delta v = 0, 1, 2$ sequence bands. The data is collected for a variety of time delays (0.25 to 40 μs) between the ablation laser (IR) and the probe (dye) laser as well as at different distances from the target. Measurements are obtained with hot

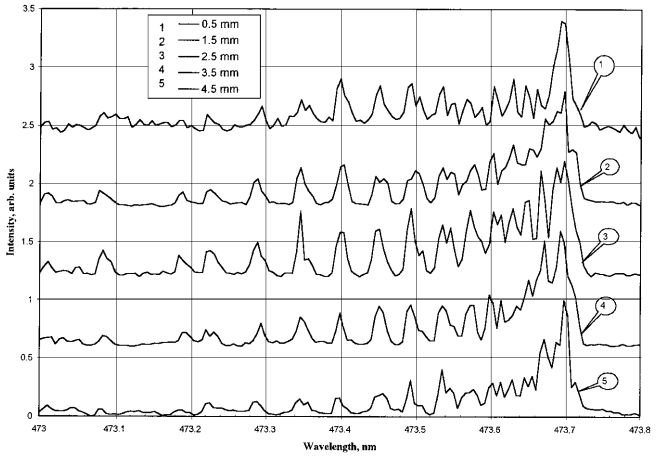

Fig. 13. Normalized hot-oven LIF data for fluorescence collection at different distances from the target at a time delay of 1 μs. Only the P-branch is shown for comparison

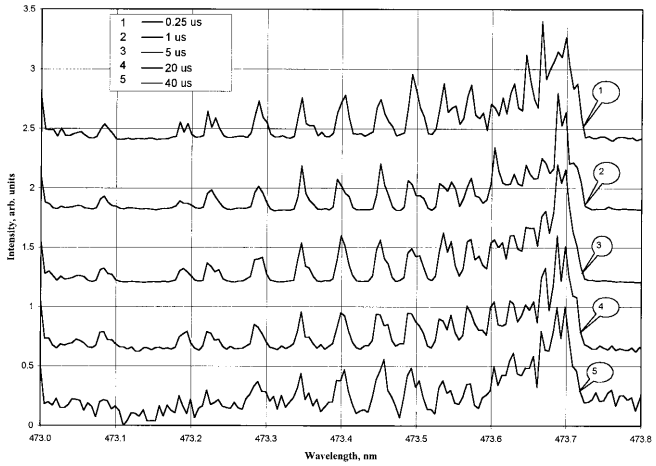

Fig. 14. Normalized hot-oven LIF data for different time delays between the ablation laser and the probe (dye) laser at a distance of 3.5 mm

and cold oven conditions. The LIF data is then compared with computed spectra [26] to estimate rotational and vibrational temperatures. The variations of the spectra with distance and time delays are shown in Figs. 13 and 14. These are corrected for dye laser energy variation and are normalized. Actual band head intensities are given in Tables 1 and 2. Comparison of the hot-oven and cold-oven measurements with computations, essentially yielded temperatures close to that of the oven. The comparison of the hot-oven data taken with a 20-μs delay at a distance of 3.5 mm is shown in Fig. 15 which indicates rotational temperature close to 1500 K. Similar data taken with cold oven yielded a temperature close to 300 K.

Table 1. Variation of LIF intensity for different time delays between the ablation laser and the probe laser

Time delay /μs	Bandhead intensity /arb. units
0.25	4.50
1.00	4.50
5.00	6.00
20.00	2.00
40.00	0.25

Table 2. Variation of LIF intensity for different distances from the target

Distance of the target from the optic axis /mm	Bandhead intensity /arb. units
0.5	1.0
1.5	6.0
2.5	5.5
3.5	4.3
4.5	2.3

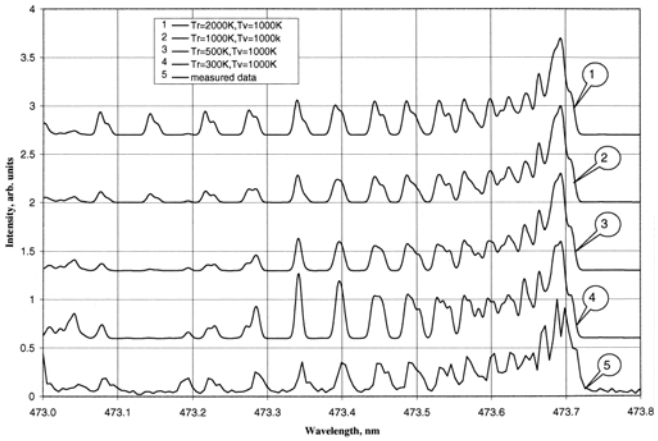

Fig. 15. Comparison of LIF data (time delay of 20 μs, at a distance of 3.5 mm) with computed spectra. Note the change in the envelope around 473.3 to 473.4 nm and relative intensities of other P-branch lines

2.5 Plume images

Two sets of ICCD images shown in Figs. 16 and 17 were taken (for the cold and hot oven) by averaging ten laser pulses with the two-laser operation. The plume image in Fig. 17 at

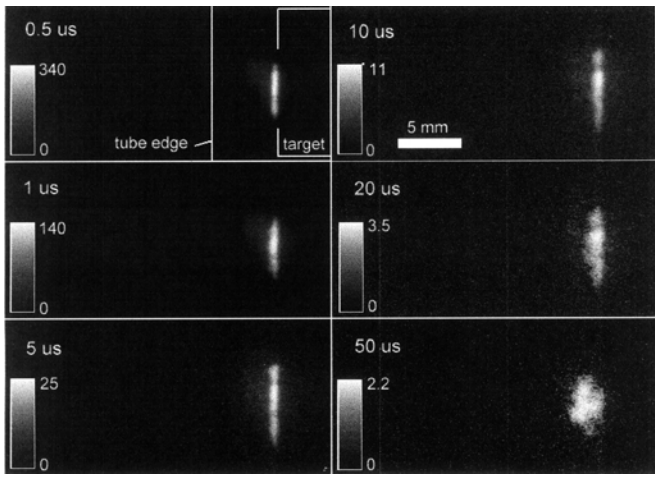

Fig. 16. Images of the plume inside the cold oven (300 K) taken with ICCD using 510 nm and notch filters. The gate width used is 12 ns and delay times are from 0.5 to 100 μs. Intensity on each snapshot is normalized, and intensity range (in arbitrary units) is shown on colorbars. Target and inner quartz tube are outlined on the first snapshot

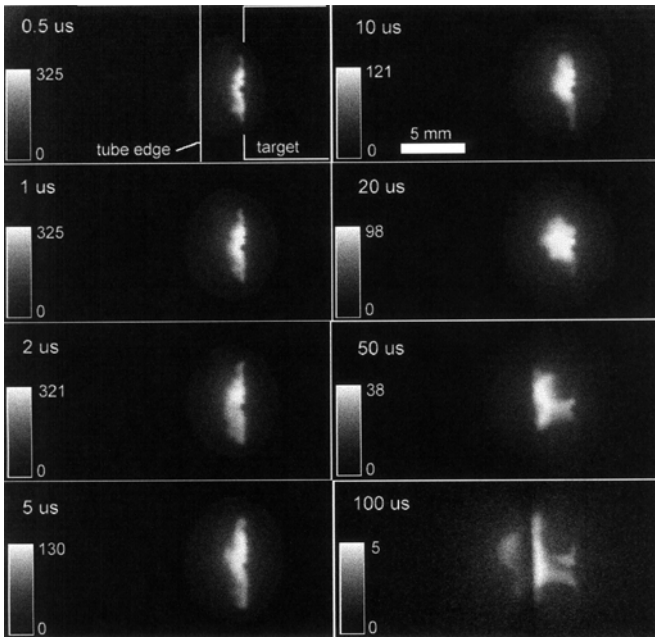

Fig. 17. Images of the plume in the hot oven (1473 K); gate width 12 ns and delay times of 0.5 to 100 μs. Notice about half of the plume inside the inner tube for 100-μs shot

50-μs delay time is partially blocked by the edge of the inner tube and the shadow is discernable in 100-μs shots. These images show that the target surface is nonuniform because of prior ablation. There seems to be a redistribution of C_2 both spatially and temporally which confirms our passive emission and transient measurements. Note that according to our spectral measurements, C_2 intensity is diminished considerably after a 10-μs delay and the plume image essentially reflects a background continuum as noted in Sect. 2.3. Also, after 20 μs, the plume in the cold-oven case seems to expand with an average velocity of 25 m/s which seems to almost double when the oven is on. When we compare these images with similar ones taken by Geohegan's group, we do not notice any of the "shock-reflection" that was reported [27]. These differences could be due to the higher pulse energy as well as photon energy used in their experiments.

3 Discussion and conclusions

The passive emission data was useful in identification of C_2 and C_3 in the plume as well as hot particles. The limitation of spatial resolution may be responsible for the current state of an "averaged" data related to temperature and populations. However, the time evolution of some of the spectral features can be used in building a chemical model similar to that proposed for C_{60} formation [16]. The LIF data yielded rotational and vibrational temperatures close to that of the oven as compared to much higher temperatures obtained from the passive emission data. This requires further investigation. The passive emission data reflects the excited state populations which are essentially determined by the chemical reactions that produce C_2 in the excited state, $\mathrm{d}\,^3\Pi_g$. In contrast, the ground state C_2 ($\mathrm{a}\,^3\Pi_u$ @716 cm^{-1}), monitored by the LIF may be in thermal equilibrium with its surroundings. The transient data taken at different distances from the target (Sect. 2.3) shows that the plume consistently moves more slowly when the target is closer to the inner tube. Also, the plume moves faster and lasts much longer at higher temperatures. The increase in velocity is expected and may be due to the lower density of the plume and purge gas (argon) as well as augmented free convection at higher temperatures. These observations are corroborated by the ICCD images (Sect. 2.5) which clearly show a smaller and slow-moving plume at cold temperatures. The confinement of the plume in the inner tube may be playing an important role in better yields when the inner tube in place as reported in [12]. It is essential to start modeling the chemical reactions incorporating the fluid mechanics to help understand the complex growth of carbon nanotubes. Also, other means of monitoring the species by techniques such as four-wave mixing and mass spectrometry may prove useful in tracking the nanotube growth. The planned parametric study to correlate the spectral measurements with quality and quantity of SWNT production will help progress towards bulk production methods; enabling more rapid investigations of nanotube applications.

Acknowledgements. The help and encouragement from Professor Richard Smalley's group, especially Andy Rinzler (currently at University of Florida) is greatly appreciated. Authors would acknowledge Tom Leimkuehler in collecting LIF data and Jim Hornkohl in LIF data analysis.

References

1. C. Dekker: Phys. Today **52**, 22 (1999)
2. S. Frank, P. Poncharal, Z.L. Wang, W.A. de Heer: Science **280**, 1744 (1998)
3. P.M. Ajayan, O. Stephan, Ph. Redlich, C. Coltrex: Nature **375**, 564 (1995)
4. B.I. Yakobson, R.E. Smalley: Am. Scientist **85**, 324 (1997)
5. A.C. Dillon, K.M. Jones, T.A. Bekkendahl, C.H. Kiang, D.S. Bethune, M.J. Heben: Nature **386**, 377 (1997)
6. Y. Ye, C.C. Ahn, C. Witham, B. Fultz, J. Liu, A.G. Rinzler, D. Colbert, K. Smith, R.E. Smalley: Appl. Phy. Lett. (1999) TS[b]
7. C. Journet, W.K. Maser, P. Bernier, A. Loiseau, M. Lamy de la Chapelle, S. Lefrant, P. Deniard, R. Lee, J.E. Fischer: Nature **388**, 756 (1998)
8. www.carbolex.com
9. Z.F. Ren, Z.P. Huang, J.W. Xu, J.H. Wang: APS Centennial meeting, March 1999, Atlanta, GA, Bull. Am. Phys. Soc. **44**, 420 (1999)
10. H.M. Cheng, F. Li, X. Sun, S.D.M. Brown, M.A. Pimenta, A. Marucci, G. Dresselhaus, M.S. Dresselhaus: Chem. Phys. Lett. **289**, 602 (1998)
11. T. Guo, P. Nikolaev, A. Thess, D.T. Colbert, R.E. Smalley: Chem. Phys. Lett. **243**, 49 (1995)
12. A.G. Rinzler, J. Liu, H. Dai, P. Nikolaev, C.B. Huffman, F.J. Rodriguez-Marcias, P.J. Boul, A.H. Liu, D. Heymann, D.T. Colbert, R.S. Lee, J.E. Fischer, A.M. Rao, P.C. Eklund, R.E. Smalley: Appl. Phys. A **67**, 29 (1998)
13. D.B. Geohegan: Oak Ridge National Laboratory, Tennessee (Private Communication)
14. A.C. Dillon, P.A. Parilla, K.M. Jones, G. Riker, M.J. Heben: Proceedings of Spring 1998 MRS Meeting, Symposium on Advances in Laser Ablation of Materials, April 13–16, 1998, San Francisco, California
15. W.K. Maser, E. Munoz, A.M. benito, M.T. Martinez, G.F. de la Fuente, Y. Maniette, E. Anglaret, J.-L. Sauvajol: Chem. Phys. Lett. **292**, 587 (1998)
16. A.V. Krestinin, A.P. Moravsky: Chem. Phys. Lett. **286**, 479 (1998)
17. E.G. Gamaly, T.W. Ebbesen: Phys. Rev. B **52**, 2083 (1995)
18. S. Bandow, S. Asaka, Y. Saito, A.M. Rao, L. Grigorian, E. Richter, P.C. Eklund: Phys. Rev. Lett. **80**, 3779 (1998)
19. S. Suzuki, Y. Ohtsuka, D. Kasuya, T. Ishigaki, H. Kataura, Y. Achiba: APS Centennial meeting, March 1999, Atlanta, GA, Bull. Am. Phys. Soc. **44**, 1433 (1999)

TS[b] Please add volume- and pagenumber.

Editor's or typesetter's annotations (will be removed before the final TEX run)

20. S. Arepalli, C.D. Scott: Chem Phys. Lett. **302**, 139 (1999)
21. S. Arepalli, C.D. Scott: Proc. of International Conference on Integrated Nano/Microtechnology for Space Applications, Houston, TX, Nov. 1998; paper # 37 (1998)
22. L.L. Danylewych, R.W. Nicholls: Proc. Royal Soc. A **339**, 197 (1974)
23. E.A. Rohlfing: J. Chem. Phys. **89**, 6103 (1988)
24. C.D. Scott, H.E. Blackwell, S. Arepalli, M.A. Akundi: J. Thermophys. Heat Transfer **12**, 457 (1998)
25. M. Yudasaka, T. Komatsu, T. Ichihashi, Y. Achiba, S. Iijima: J. Phys. Chem. B **102**, 4892 (1998)
26. J. Hornkohl: Tennessee Space Institute, Tullahoma, Tennessee (private communication)
27. D.B. Geohegan, A.A. Puretzky, R.L. Hettich, X.-Y. Zheng, R.E. Haufler, R.N. Compton: Advanced materials'93, IV/Laser and Ion beam Modification of Materials, ed. by I. Yamada, et al., IUMRS-ICAM Conference, Trans. Mat. Res. Soc. Jpn. **17**, 349 (1994)